AFRL-AFOSR-VA-TR-2019-0232

Regeneration of Structural Materials in Adaptive Response to External Stimuli

Nancy Sottos
UNIVERSITY OF ILLINOIS

08/01/2019
Final Report

Air Force Research Laboratory
AF Office Of Scientific Research (AFOSR)/ RTB2
Arlington, Virginia 22203
Air Force Materiel Command

REPORT DOCUMENTATION PAGE

Form Approved
OMB No. 0704-0188

1. REPORT DATE *(DD-MM-YYYY)*
08-08-2019

2. REPORT TYPE
Final Performance

3. DATES COVERED *(From - To)*
01 May 2015 to 30 Apr 2019

4. TITLE AND SUBTITLE
Regeneration of Structural Materials in Adaptive Response to External Stimuli

5a. CONTRACT NUMBER

5b. GRANT NUMBER
FA9550-15-1-0087

5c. PROGRAM ELEMENT NUMBER
61102F

6. AUTHOR(S)
Nancy Sottos

5d. PROJECT NUMBER

5e. TASK NUMBER

5f. WORK UNIT NUMBER

7. PERFORMING ORGANIZATION NAME(S) AND ADDRESS(ES)
UNIVERSITY OF ILLINOIS
506 S WRIGHT STREET SUITE 364
URBANA, IL 61801-3649 US

8. PERFORMING ORGANIZATION REPORT NUMBER

9. SPONSORING/MONITORING AGENCY NAME(S) AND ADDRESS(ES)
AF Office of Scientific Research
875 N. Randolph St. Room 3112
Arlington, VA 22203

10. SPONSOR/MONITOR'S ACRONYM(S)
AFRL/AFOSR RTB2

11. SPONSOR/MONITOR'S REPORT NUMBER(S)
AFRL-AFOSR-VA-TR-2019-0232

12. DISTRIBUTION/AVAILABILITY STATEMENT
A DISTRIBUTION UNLIMITED: PB Public Release

13. SUPPLEMENTARY NOTES

14. ABSTRACT

The research performed under AFOSR grant FA9550-15-1-0087, Regeneration of Structural Materials in Adaptive Response to External Stimuli, focuses on the development of regenerative structural materials in response to environmental stimuli. This research is also part of the AFOSR Center of Excellence on Self-Healing Regeneration and Remodeling (grant FA9550-16-1-0017). The program is highly interdisciplinary and collaborative, spanning materials science, chemistry, mechanics and advanced modeling at the University of Illinois and the University of Chicago. A total of 25 archival papers were published, including high impact publications in Nature and Nature Chemistry. Two patent applications were published. The research in this program addresses the entire life cycle of multifunctional composites materials, from developing new methods of manufacturing, to healing and regeneration following extensive damage, to imparting dynamic adaptability and ultimately remodeling of polymeric materials. The research is divided into two main themes: (1) Dynamically adaptable vascular remodeling and growth of polymers and (2) Rapid manufacturing of multifunctional composites. Key technical accomplishments from each theme are summarized in this report.

15. SUBJECT TERMS
Self-Healing, Regeneration, Remodeling, Microvascular composites, dynamic polymers

16. SECURITY CLASSIFICATION OF:			**17. LIMITATION OF ABSTRACT**	**18. NUMBER OF PAGES**	**19a. NAME OF RESPONSIBLE PERSON**
a. REPORT	**b. ABSTRACT**	**c. THIS PAGE**			LEE, BYUNG
Unclassified	Unclassified	Unclassified	UU		

					19b. TELEPHONE NUMBER *(Include area code)* 703-696-8483

Standard Form 298 (Rev. 8/98)
Prescribed by ANSI Std. Z39.18

DISTRIBUTION A: Distribution approved for public release

Regeneration of Structural Materials in Adaptive Response to External Stimuli

Award No. FA9550-15-1-0087
FINAL REPORT

July 31, 2019

UNIVERSITY OF ILLINOIS AT URBANA-CHAMPAIGN
Nancy Sottos (PI), Philippe Geubelle, Jeffrey Moore

UNIVERSITY OF CHICAGO
Aaron Esser-Kahn

SUMMARY

The research performed under AFOSR grant FA9550-15-1-0087, *Regeneration of Structural Materials in Adaptive Response to External Stimuli*, focuses on the development of regenerative structural materials in response to environmental stimuli. This research is also part of the AFOSR Center of Excellence on Self-Healing Regeneration and Remodeling (grant FA9550-16-1-0017). The program is highly interdisciplinary and collaborative, spanning materials science, chemistry, mechanics and advanced modeling at the University of Illinois and the University of Chicago. A total of 25 archival papers were published, including high impact publications in *Nature and Nature Chemistry*. Two patent applications were published. The research in this program addresses the entire life cycle of multifunctional composites materials, from developing new methods of manufacturing, to healing and regeneration following extensive damage, to imparting dynamic adaptability and ultimately remodeling of polymeric materials (Fig. 1). The research is divided into two main themes: (1) Dynamically adaptable vascular remodeling and growth of polymers and (2) Rapid manufacturing of multifunctional composites. Key technical accomplishments from each theme are summarized in this report.

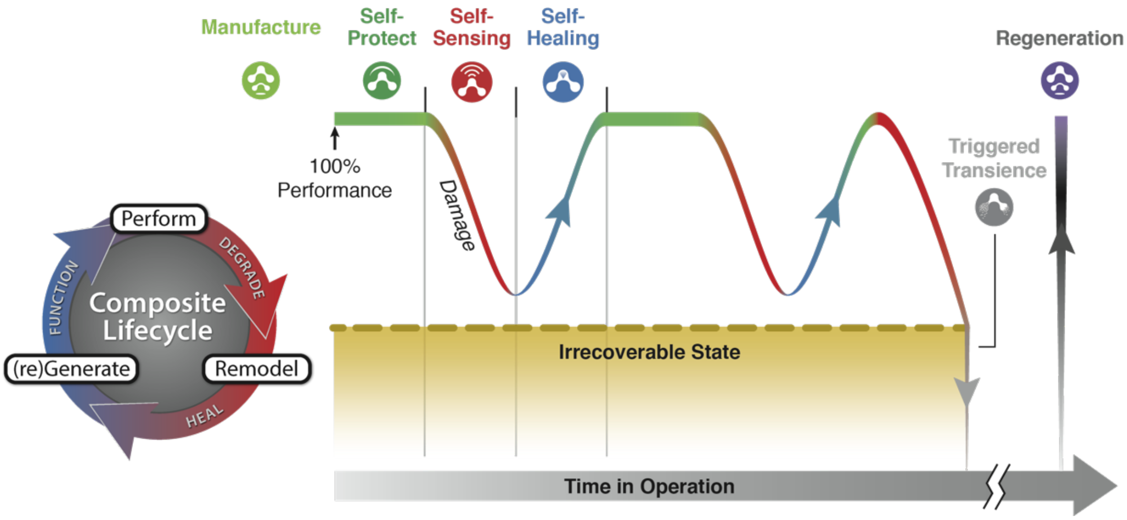

Figure 1. *The Center of Excellence in Self-Healing, Regeneration, and Structural Remodeling addresses the entire lifecycle of multifunctional composite materials [1].*

PUBLICATIONS

1. Krull, B. P.; Gergely, R. C. R.; Santa Cruz, W. A.; Fedonina, Y. I.; Patrick, J. F.; Moore, J. S.; White, S. R.; Sottos, N. R. Strategies for Volumetric Recovery of Large Scale Damage in Polymers. *Advanced Functional Materials*, **26**, 4561-4569 (2016).
2. Robertson, I. D.; Pruitt, E. L.; Moore, J. S. Frontal Ring-Opening Metathesis Polymerization of Exo-Dicyclopentadiene for Low Catalyst Loadings. *ACS Macro Letters*, **5**, 593–596 (2016).
3. Patrick, J.F., Robb, M.J., Sottos, N.R., Moore, J.S. and White, S.R., Polymers with autonomous life-cycle control, *Nature*, **540**, 363-370 (2016).
4. Coppola, A.M., Warpinski, L.G., Murray, S.P., Sottos, N.R. and White, S.R., Survival of actively cooled microvascular polymer matrix composites under sustained thermomechanical loading, *Composites Part A: Applied Science and Manufacturing*, **82**, 170-179 (2016).
5. Robertson, I. D.; Dean, L. M.; Rudebusch, G. E.; Sottos, N. R.; White, S. R.; Moore, J. S. Alkyl Phosphite Inhibitors for Frontal Ring-Opening Metathesis Polymerization Greatly Increase Pot Life. *ACS Macro Letters*, **6**, 609-612 (2017).
6. Mohapatra, H.; Kleiman, M.; Esser-Kahn, A. Mechanically Controlled Radical Polymerization Initiated by Ultrasound. *Nature Chemistry*, **9**, 135-139 (2017).
7. Patrick, J.F., Krull, B.P., Garg, M., Mangun, C.L., Moore, J.S., Sottos, N.R., and White, S.R., Robust Sacrificial Polymer Templates for 3D Interconnected Microvasculature in Fiber-Reinforced Composites, *Composites Part A*, **100**, 361-370 (2017).
8. Gergely, R.C.R.; Rossol, M.N.; Tsubaki, S.; Wang, J.; Sottos, N.R.; White, S.R. A Microvascular System of the Autonomous Regeneration of Large Scale Damage in Polymeric Coatings, *Advanced Engineering Materials*. 1700319 (2017).
9. Gergely, R.C.R.; Sottos, N.R.; White, S.R. Regenerative Polymeric Coatings Enabled by Pressure Responsive Surface Valves. *Advanced Engineering Materials*, 1700308 (2017).
10. Pety, S.J., Chia, P.X.L., Carrington, S.M., and White, S.R., Active Cooling of Microvascular Composites for Battery Packaging, Smart Materials and Structures, 26, 105004 (2017).
11. Moneypenny, T.P., Liu, H.Y., Yang, A., Robertson, I.D., Moore, J.S., Grubbs-Inspired Metathesis in the Moore Group, Journal of Polymer Science Part A- Polymer Chemistry, 55, 2935-2948 (2017).
12. Mohaptra, H.; Ayarza, J.; Sanders, E. C.; Scheuermann, A. M.; Griffin, P. J.; Esser-Kahn, A. P. Ultrasound Promoted Step-Growth Polymerization and Polymer Crosslinking Via Copper Catalyzed Azide–Alkyne “Click” Reaction. *Angew. Chem. Int. Ed.*, 57,11208-11212 (2018).
13. Dean, L.M.; Krull, B.P.; Li, K.R.; Fedonina, Y.I.; White, S.R.; Sottos, N.R. Enhanced Mixing of Microvascular Self-Healing Reagents Using Segmented Gas−Liquid Flow. *Applied Materials and Interfaces*, 10, 32659-32667 (2018).
14. Gergeley, R.C.R.; Santa Cruz, W.A.; Krull, B.P.; Pruitt, E.L.; Wang, J.; Sottos, N.R.; White, S.R. Biomimetics: Restoration of Impact Damage in Polymers via a Hybrid

Microcapsule–Microvascular Self-Healing System. *Advanced Functional Materials*, 28, 1704197 (2018).

15. Liu, H.; Nelson, A. Z.; Ren, Y.; Yang, K.; Ewoldt, R. H.; Moore, J. S. Dynamic Remodeling of Covalent Networks via Ring-Opening Metathesis Polymerization. *ACS Macro Lett. 7*, 933-937 (2018).
16. Goli, E.; Robertson I.D.; Geubelle, P.H.; Moore, J.S. Frontal Polymerization of Dicyclopentadiene: A Numerical Study. *The Journal of Physical Chemistry B*, 122, 4583-4591 (2018).
17. Brubaker, K.; Kleiman, M.; Hernandez, L.; Bhattacharjee, A.; Esser-Kahn, A. P. Structural remodeling of polymeric material via diffusion controlled polymerization and chain scission. *Chemistry of Materials*, 30, 8126-8133 (2018).
18. Brubaker, K.; Garewal, A., Steinhardt, R.C., Esser-Kahn, A.P. Bio-inspired counter-current for enrichment of solutes. *Nature Communications*, 9,736 (2018).
19. Robertson, I.D.; Yourdkhani, M.; Centellas, P.J.; Aw, J.E.; Ivanoff, D.G.; Goli, E.; Lloyd, E.M.; Dean, L.M.; Sottos, N.R.; Geubelle, P.H.; Moore, J.S. Rapid energy-efficient manufacturing of polymers and composites via frontal polymerization. *Nature*, 557, 223-227 (2018).
20. Lloyd, E. M., Lopez Hernandez, H.L.; Yourdkhani, M.; Zen, E. K.; Sottos, N. R.; Moore, J. S.; White, S. R. Fully Recyclable Metastable Polymers and Composites. *Chemistry of Materials*, 31, 398-406 (2019).
21. Goli, E.; Robertson, I. D.; Agarwal, H., Pruitt, E., Grolman, J.M., Geubelle, P.H.; Moore, J.S. Frontal Polymerization Accelerated by Continuous Conductive Elements. *Journal of Applied Polymer Science*, 136, 47418 (2019).
22. Shin, J., Sung, J., Kang, M., Xie, X., Lee, B., Lee, K.M., White, T.J, Leal, C., Sottos, N.R., Braun, P.V., Cahill, D.G., Light-triggered Thermal Conductivity Switching in Azobenzen Polymers, *Proceedings of the National Academy of Sciences*, 116, 5973-5978 (2019).
23. Lopez Hernandez, H.L.; Takekuma, S.K., Mejia, EB, Plantz, CL, Sottos, N.R., Moore, J.S., and White, S.R. Processing-dependent mechanical properties of solvent cast cyclic polyphthalaldehyde, *Polymer*, 162, 29-34 (2019).
24. Liu, H., Wei, H. and Moore, J.S., Frontal Ring-Opening Metathesis Copolymerization: Deviation of Front Velocity from Mixing Rules, *ACS Macro Letters*, 8, 846-851 (2019).
25. Wang Z, Ayarza J, Esser-Kahn AP. Mechanically Initiated, Bulk Free Radical Polymerization. *Angewandte Chemie International Edition*, ASAP.

PATENTS

1. Robertson, I. D.; Sottos, N. R.; White, S. R.; Moore, J. S. “Frontal Polymerization for Fiber-Reinforced Composites” (2016) U.S. Patent Application No. 15/462,458.
2. Robertson, I. D.; Aw, J. E.; Sottos, N. R.; White, S. R.; Moore, J. S. “3D Printing of Thermoset Polymers and Composites” (2017) U.S. Patent Application No. 15/979,029

RESEARCH RESULTS

1. Synthetic Regeneration and Remodeling

1.1. Mechanochemical Materials Remodeling

We have fabricated novel polymeric materials that respond to mechanical force and strengthen themselves. In particular, we have developed polymerization and crosslinking reactions that can be activated and controlled by means of the piezoelectric effect [2-4]. We have shown that piezochemical reduction of a Cu^{II}-based pre-catalyst initiates a step-growth polymerization via a copper catalyzed azide-alkyne cycloaddition (copper “click” reaction) to form a linear polytriazole. We then expanded our toolset of mechano-click reactions by synthesizing a linear polyurethane with pendant azide groups that is crosslinked mechanochemically using the same chemistry to form a solid organogel (Fig. 2). We are working to apply these mechano-click reactions in solid composites, thus showing that this chemistry can be used to effectively strengthen a polymeric material.

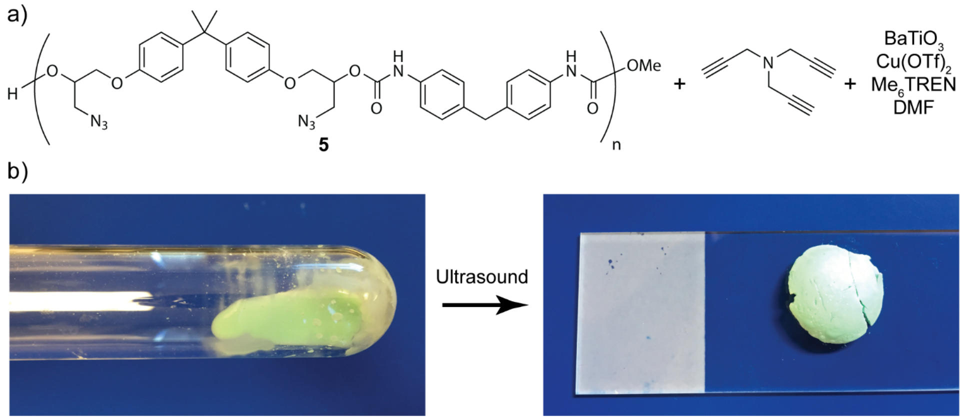

Figure 2. *Ultrasound mediated polymer crosslinking using mechano-click reaction (a) Components of pre-crosslinked polyurethane-trialkyne mixture; (b) Photographs depicting the starting reaction mixture (left) and the solid polymer gel obtained after sonication (right).*

1.2 Structural Remodeling

We have developed a synthetic system that uses reaction and diffusion to both grow new material via polymerization and remove material through polymer chain breakage - mimicking the process of bone remodeling in a synthetic system [5-8]. We first demonstrated reaction-diffusion based control of irreversible etching through the use of an etchant and a diffusible inhibitor [8]. Tetrabutylammonium fluoride (TBAF) was used to break the Si-O-Si bonds of poly-dimethylsiloxane (PDMS) and remove material from the surface in areas of high TBAF concentration. Using triethoxy methyl silane (TEMS) allowed the location and rate of etching around a channel to be controlled. While affording diffusion-based control of structure, the TBAF/TEMS system was limited to removing existing material. In order to add material, we initiated polymerization of octamethylcyclotetrasiloxane with TBAF, thus establishing a competition between polymerization and F^- mediated chain scission. Controlling this competition allows a dynamic structural equilibrium to be established where the polymer growth rate (addition of material) is balanced with the polymer scission rate (removal of material) on the initial structure. Use of a small amount of D4 dimer (D4-D4), linked via a methylene bridge, results in a cross-linked, structurally stable material. The resulting material is chemically dynamic and capable of reshaping its structure in response to diffusion gradients, facilitating both structural changes and structural homeostasis, approximating the mechanism of bone remodeling (Fig. 3). Adjusting the conditions of the reactions taking place, features can be added to and removed from a surface dynamically using the same reagents.

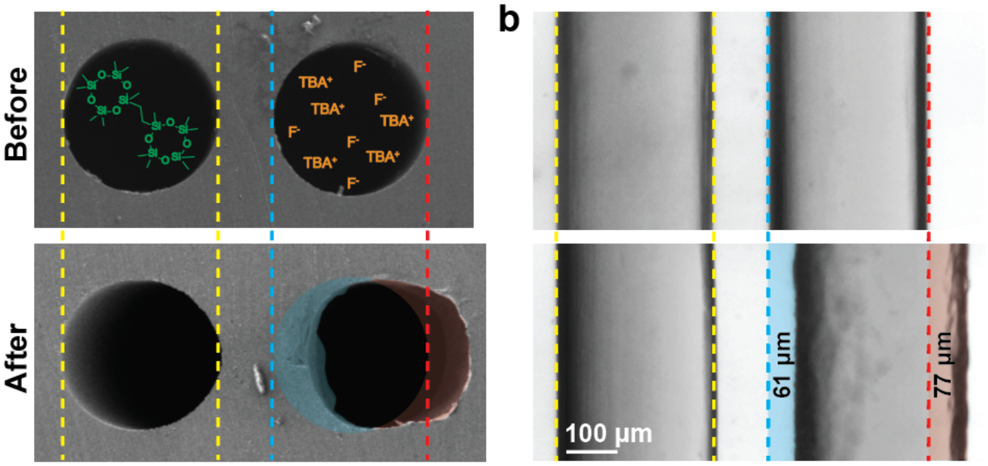

Figure 3. *Concurrent growth and removal. Cross section (**a**) and top down (**b**) view of a shifting channel. Concurrent growth (blue) and removal (red) caused a shift of the channel through space, maintaining the general shape and size.*

1.3 Regeneration of Large-Scale Damage

Our team developed a novel two-stage chemistry for the restoration of lost material due to large scale damage in thermoset polymers [9-10]. Unlike traditional self-healing approaches, which are limited to the length scale of microcracks, the two-stage chemistry circumvents gravity-driven loss of liquid healing agents at a damage site, thus enabling autonomous self-healing of millimeter scale damage. Liquid healing agents are delivered from an external reservoir to a damage site through a microvascular network. Upon mixing, the two reactive fluids rapidly form a self-supporting gel which spans the width of the damage. The swelling agent in the gel is liquid monomer, which subsequently polymerizes to form a structural material (Fig. 4a).

We introduced the concept of segmented gas-liquid flow for improving the mixing of microvascular healing agents [11]. In segmented gas-liquid flow, gas bubbles and liquid slugs flow concurrently as discrete segments through a microchannel (Fig 4b). We successfully implemented segmented gas-liquid flow to deliver two-stage healing agents for the restoration of large-scale damage in thermoset polymers (Fig. 4c). We found that the mixing of the healing agents at a damage site is improved by using segmented gas-liquid flow compared to alternative microvascular delivery strategies. We also increased the maximum damage size that could be healed by 25% compared to laminar single-phase flow (Fig. 4c).

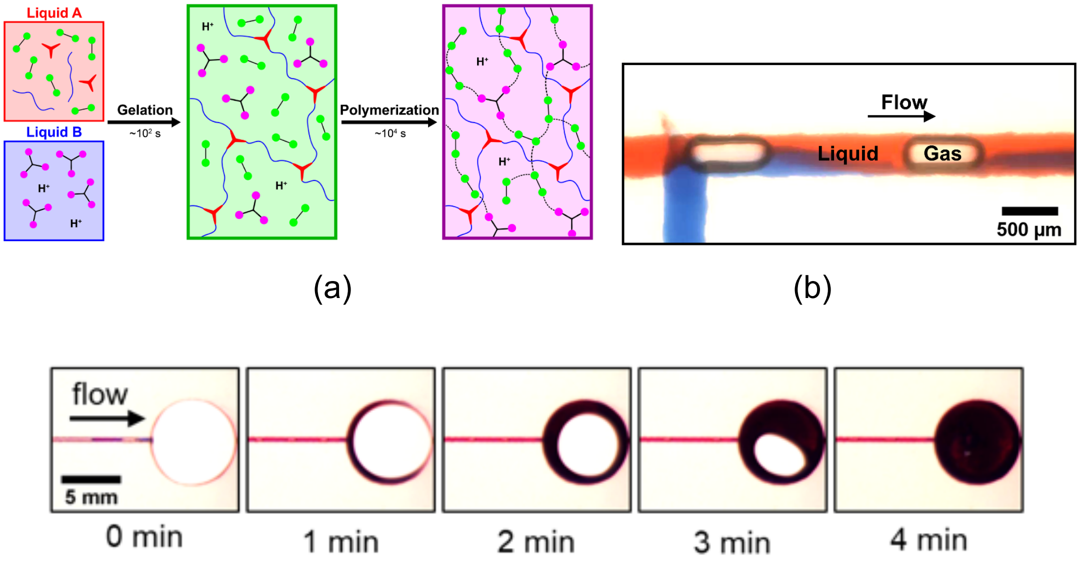

(a)

(b)

(c)

Figure 4. *Schematic of two-stage damage restoration in thermoset polymers. (a) Liquid healing agents are segregated into two solutions. Upon mixing, the first stage gelation reaction occurs on the order of seconds. The second stage polymerization reaction occurs on the order of hours to restore the structural integrity of the material. (b, c) Using segmented gas-liquid flow to deliver healing agents enhances mixing at the damage site. The healing agents form a gel scaffold which spans the damage [11].*

2. Rapid Manufacturing of Multifunctional Composites

We have developed a new manufacturing process that allows for near net-zero energy fabrication of multifunctional thermosetting polymers and composites. Our approach utilizes a frontal polymerization (FP) curing strategy, which substantially reduces manufacturing burdens by employing the enthalpy of polymerization of the monomer to provide the energy for materials synthesis, rather than requiring an external energy source [12-13]. In FP (Fig. 5), a solution of monomer and latent initiator is heated locally until the initiator is activated towards the polymerization of the monomer, producing heat from the polymerization which further drives the reaction. This reaction-diffusion (RD) system produces a propagating reaction wave that rapidly transforms the available monomer into polymer. In the simplest 1D setting, the reaction-diffusion equations describing the propagation of a polymerization front can be expressed in terms of the following coupled thermo-chemical equations,

$$\kappa \frac{\partial^2 T}{\partial x^2} + \rho H_R \frac{\partial \alpha}{\partial t} = \rho c_p \frac{\partial T}{\partial t}$$

$$\frac{\partial \alpha}{\partial t} = f(\alpha, E_a, T)$$

where α and T are the degree of cure and temperature, respectively, H_R is the heat of reaction, E_a is the activation energy, and κ, ρ and c_p respectively denote the thermal conductivity, density and specific heat of the material. The second term of the first equation corresponds to the heat generated by the exothermic reaction. The second equation describes the cure kinetics model, i.e., the evolution of the degree of cure.

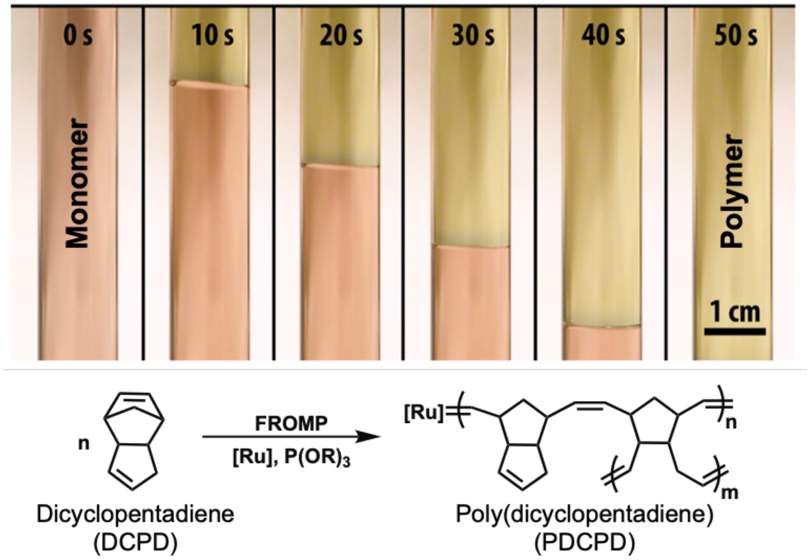

Figure 5. *Images of frontal ring opening metathesis polymerization (FROMP) of dicyclopentadiene (DCPD) [14].*

2.1 Enabling Chemistry

We invetigated the frontal ring-opening metathesis polymerization (FROMP) of dicyclopentadiene (DCPD) that exhibits the high energy density, high reactivity, relatively long pot life, and low viscosity required for the synthesis of high-performance thermosets (Fig. 5) [14]. The resulting polydicyclopentadiene (pDCPD) is a cross-linked thermoset polymer suitable for the fabrication of structural parts, owing to its high fracture toughness, stiffness, and chemical resistance.

In the past, FROMP chemistry has been severely limited by its short pot life of < 30 min [15,16]. We overcame pot life issues through the use of alkyl phosphite inhibitors, which extended the room temperature liquid processing window for FROMP of DCPD up to 30 h [17]. At room temperature, the phosphite is enthalpically favored to coordinate to the metal center of the ruthenium alkylidene, which inhibits polymerization of DCPD. At high temperature, increased entropic effects favor phosphite dissociation and enable ROMP to proceed with minimal hindrance. As a result, alkyl phosphite inhibition has revealed slow background polymerization that manifests as a liquid to gel transition, while maintaining high front velocities throughout the transition.

Trimethyl phosphite (TMP), triethyl phosphite (TEP), and tributyl phosphite (TBP) were tested as inhibitors for FROMP at a range of concentrations between 0.3 and 8 equiv (with respect to GC2) to explore their effects on frontal velocity and pot life. The concentration of GC2 in DCPD was 100 ppm in all experiments. The pot life was quantified as the time for the mixture to reach its gel point, determined as the crossover of the shear storage and shear loss moduli from isothermal (temperature = 23 °C) bulk rheology. As expected, in all cases, pot life increased as inhibitor concentration increased (Fig. 6a). However, despite their structural similarity, the three alkyl phosphites inhibited polymerization to different degrees. Samples inhibited with TBP exhibited the greatest effect. Even with 0.3 equiv of TBP, the pot life was extended by 6-fold to about 1 h. With 8 equiv of TBP, the pot life was remarkably extended to over 30 h, by far the longest FROMP pot life reported in the literature.

Frontal velocity shows an inverse trend to pot life; greater quantities of inhibitor correspondingly reduce frontal velocity (Fig. 6b). However, unlike pot life, there was essentially no difference in the effect of the three alkyl phosphites on frontal velocity. Furthermore, the magnitude of reduction in frontal velocity is significantly smaller than the magnitude of the increase in pot life. The addition of 1 equiv of TMP, TEP, or TBP reduced the frontal velocity by only about 40%, while the pot lives of these systems were increased by 700, 1500, and 2400%, respectively.

Phosphite-inhibited DCPD containing 2nd generation Grubbs' catalyst slowly transforms at room temperature from a liquid to a viscoelastic gel. Remarkably, the gelation of the monomer does not result in concomitant spontaneous polymerization, as observed with previous FROMP chemistries. Tuning the inhibitor concentration allows

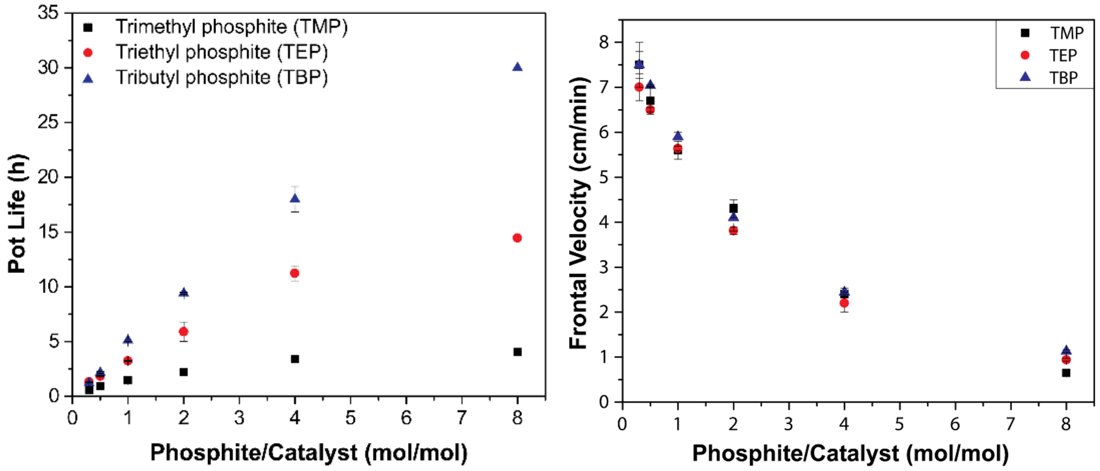

(a) (b)

Figure 6. *Effect of alkyl phosphite inhibitors on (a) pot life of FROMP solutions and (b) front velocity. Application of 8 equiv TBP to catalyst can increase pot life by >140×. Error bars are standard deviation; N =3.*

access to a range of rheological profiles between low-viscosity liquid and free-standing elastomeric gel, all of which frontally polymerize upon thermal activation. Successful control of the chemistry and rheology enabled rapid fabrication of parts with microscale features, 3D printed structures, and continuous carbon fiber-reinforced polymer (CFRP) composites with excellent mechanical properties [14].

2.2 FROMP monomer design

To obtain better mechanical properties in composite manufacturing, hotter monomers (i.e., more heat generated per unit time/volume) are highly desirable to compensate heat loss while increasing the fiber volume fraction. Thus far, only DCPD has been reported as the FROMP monomer (4). Systematic studies on other monomers not only expand the toolbox of FROMP, but also guide new monomer design that further modifies the material properties and advances the current system.

As shown in Scheme 1, we investigated thermodynamics, kinetics and frontal velocity of different strained monomers to build structure-property relationship [18]. For norbornene derivatives, there is a linear correlation between frontal velocity and heat release rate which is experimentally determined as the product of enthalpy (kJ/g), density (g/L) and rate constant (min^{-1}) of ROMP. However, the correlation is less satisfactory when considering monomers with different ring nature. A more general and accurate model that correlates frontal velocity with monomer properties is still under investigation.

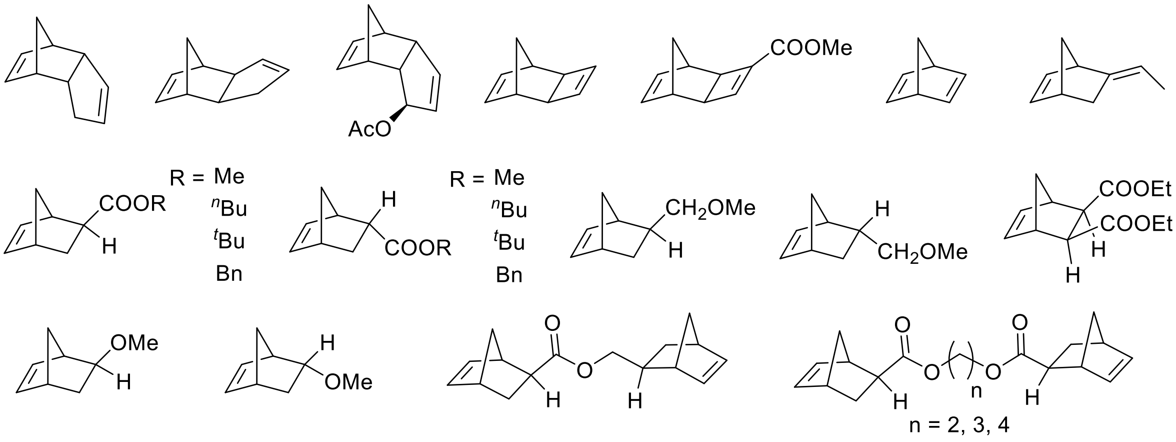

Scheme 1. *Investigated FROMP monomers.*

Copolymerization in FROMP allows for systematic modification of material properties while maintaining the benefits of our current system such as low cost of *endo*-DCPD monomer and excellent mechanical properties of PDCPD. Due to relatively low ring strain of cyclopentene, ring-opening of cyclopentenyl C=C bond is thermodynamically unfavorable (5), and the degree of cross-linking in the resulting PDCPD is low. One approach to increase cross-linking density and enhance the tensile strength is to introduce dinorbornenyl cross-linker.

Based on structure-property relationship studies of FROMP monomers, cross-linker **2** with the ester linkage is designed to possess a high front velocity, which is measured to be 0.96 mm/s, close to *endo*-DCPD (1.00 mm/s). Copolymerization of *endo*-DCPD and cross-linker **2** is expected to tune the mechanical properties while propagating at a velocity between the velocities of the two individual monomers according to the Rule of Mixtures. This assumption holds for FROMP with co-monomer **1** (Fig. 7a). However, as shown in Fig. 7b, a non-monotonic increase was observed with the increase in cross-linker loading, which does not conform to the Rule of Mixtures.

A similar response was also observed with cross-linker **3** which has a much lower frontal velocity of 0.6 mm/s (Fig. 7c). The unusual behavior is hypothesized to result from the proximity of two norbornenyl rings. This hypothesis is supported by the steady decrease in frontal velocity when copolymerizing with cross-linker **4**, where the two rings are further apart (Fig. 7d). This study not only demonstrates an alternative approach to modify material properties without compromising on frontal velocity, but also provides mechanistic insights on interactions of strained rings in FROMP.

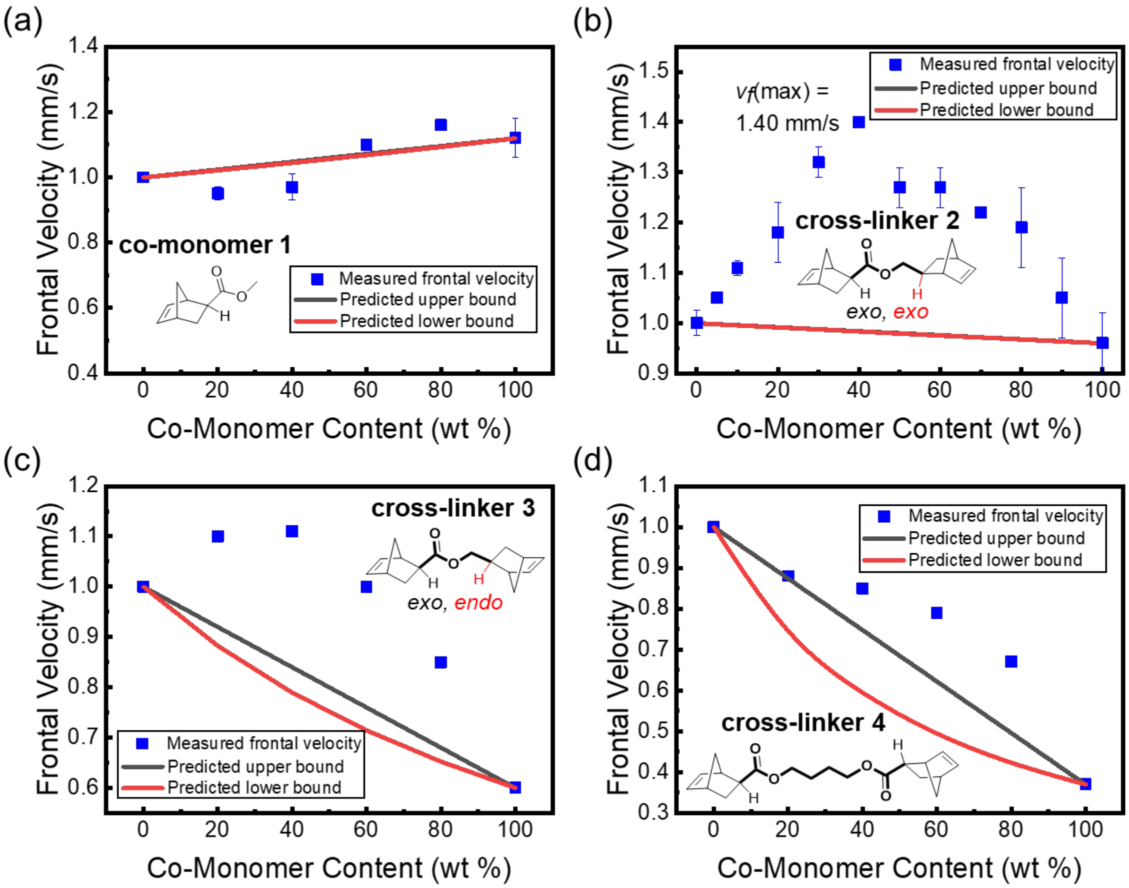

***Figure 7.** Frontal velocities in copolymerization of endo-DCPD with (a) monomer **1**, (b) cross-linker **2**, (c) cross-linker **3** and (d) cross-linker **4** at different co-monomer ratios [18].*

2.3 FP Curing of Fiber Reinforced Composites

In our demonstration of FP composite curing, we fabricated carbon fiber reinforced polymer matrix (CFRP) panels in less than 5 min by FROMP [14]. The very low viscosity of the liquid monomer at room temperatures (ca. 1.5 cP) allows for rapid infusion of the resin into high fiber volume fraction continuous fiber layups via out-of-autoclave processing techniques such as vacuum-assisted resin transfer molding (VARTM). Once resin completely infused the fabric stack, a constant electric current was applied across the resistive wire until FP initiated in the layup and then the power was turned off (Fig. 8a). A 10 cm × 20 cm CFRP panel was manufactured in two minutes, which would otherwise take more than 10 hours to cure using conventional techniques. These composites had high fiber volume fraction (ϕ =0.51) and low void content (0.2%).

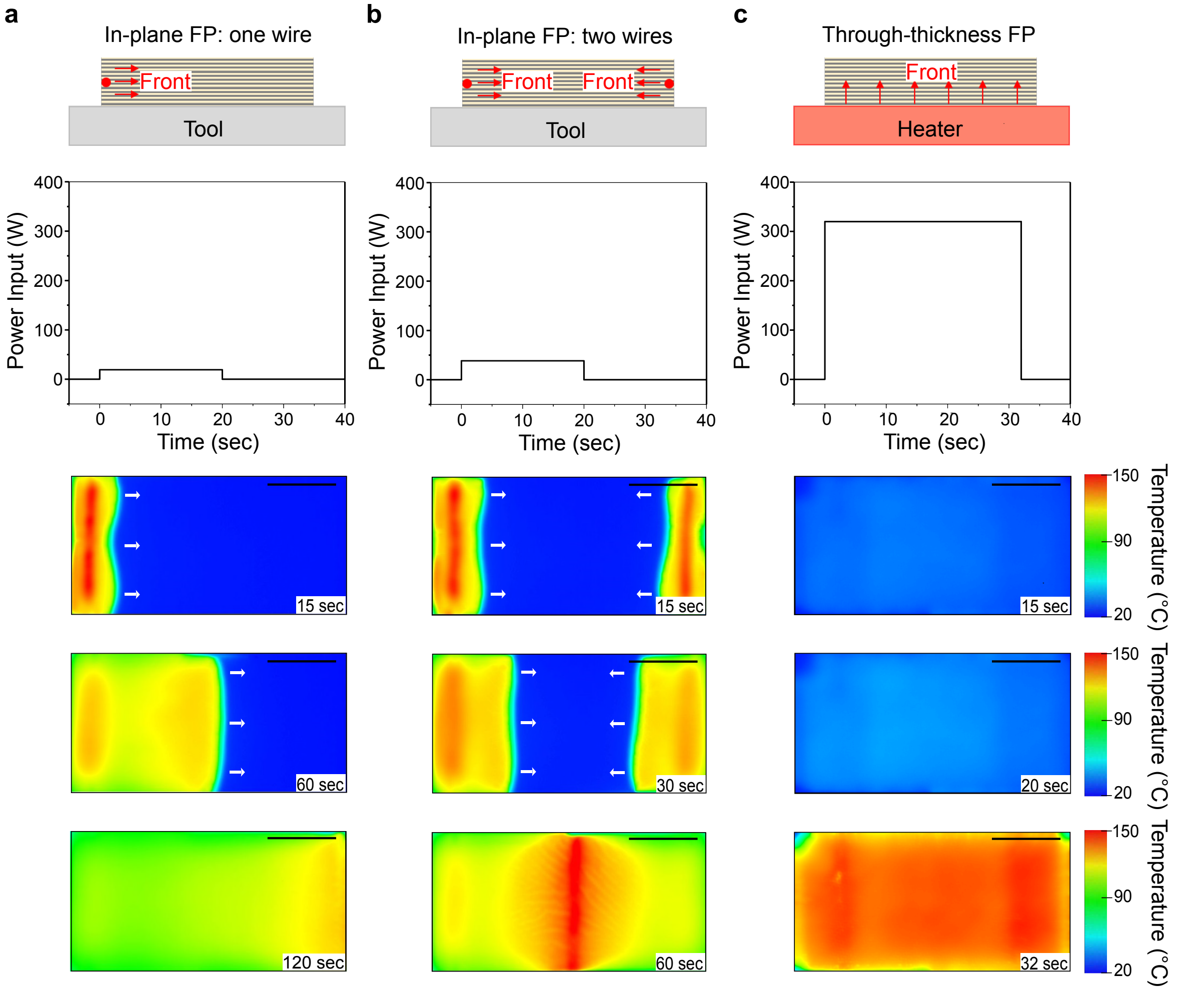

Figure 8. *FP manufacturing of CFRP. a) IR images of FP of CFRP panel produced by a single edge trigger b) Fully cured CFRP panel after 2 min. b) Mechanical properties of FRPCs produced with FP-DCPD compared to oven cure bisphenol A (BPA) epoxy [14].*

We also explored other triggering methods to further reduce the manufacturing time. Using two resistive wires (i.e. two initiation points) on opposite sides of the layup reduced the manufacturing time by half (Fig. 8b). Alternatively, a heating pad was placed underneath the layup to cure the composite through the thickness; using this curing strategy, we could manufacture a 10 cm × 20 cm panel in 32 s (Fig. 8c). In the two-point trigger layup (Fig. 8b), we measured a thermal spike where the two fronts merged via *in situ* infrared imaging. Post-fabrication, we also measured non-uniform panel thickness and increased voids at this same merged front interface. Placement of a thermally conductive constraint over the merged front region serves to minimize void formation. Additionally, the metal constraint aids in quenching the thermal spike and improving thickness uniformity at the merged interface.

We investigated the effect conductive carbon fibers on the frontal polymerization (FP) of dicyclopentadiene (DCPD). A parametric study for the front temperature and velocity with fiber volume fractions from 0 – 47% was conducted (Fig. 9a and 9b). Liquid resin was infused into a unidirectional continuous fiber layup using resin transfer molding (RTM) processing technique. The FP reaction was triggered via point source through an external power source.

Fabrication of higher volume fraction composites required additional compression of the fabric preform and vacuum-assisted resin transfer molding (VARTM) processing technique. The composite layup (Fig. 10a) used a continuous fabric preform containing a resistive heater. Once infused with the liquid resin, a constant electric current was applied to a resistive heater embedded in the layup which triggered the FP reaction and then power was turned off. We have demonstrated successful manufacturing of high-performance FRPCs with high volume fractions up to 63% and low void content (below 0.1%) (Figure10b).

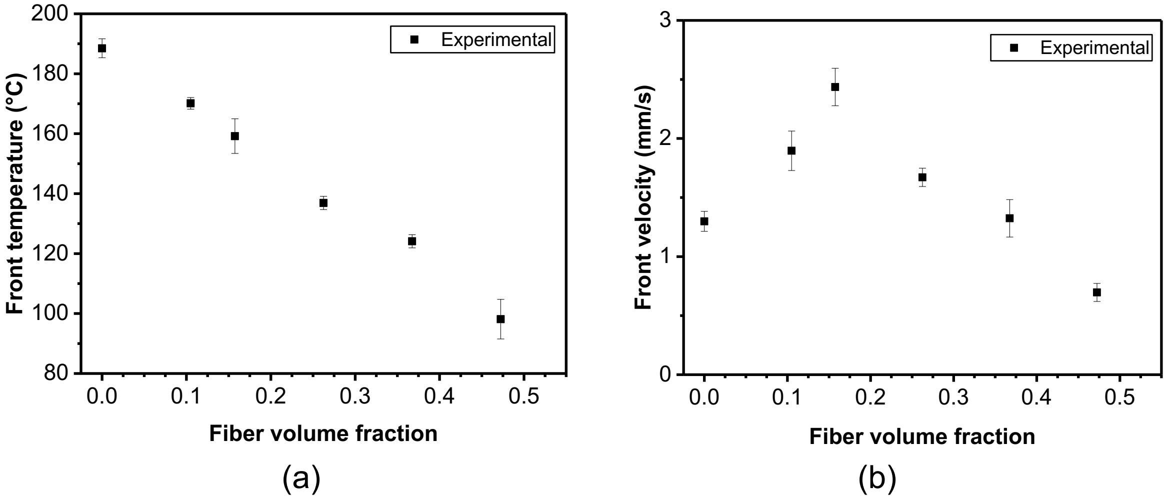

(a) (b)

Figure 9. *a) Experimental characterization of front temperature and b) front velocity with varying fiber volume fractions.*

Finally, we characterized the mechanical properties and fracture toughness of neat FP-DCPD and FRPC FP-DCPD panels and compared to the bulk-cured DCPD as well as an aerospace-grade epoxy counterparts (Fig. 11). The tensile properties (i.e. stiffness and strength) of FP-cured neat resin panels were comparable to those of bulk-cured panels.

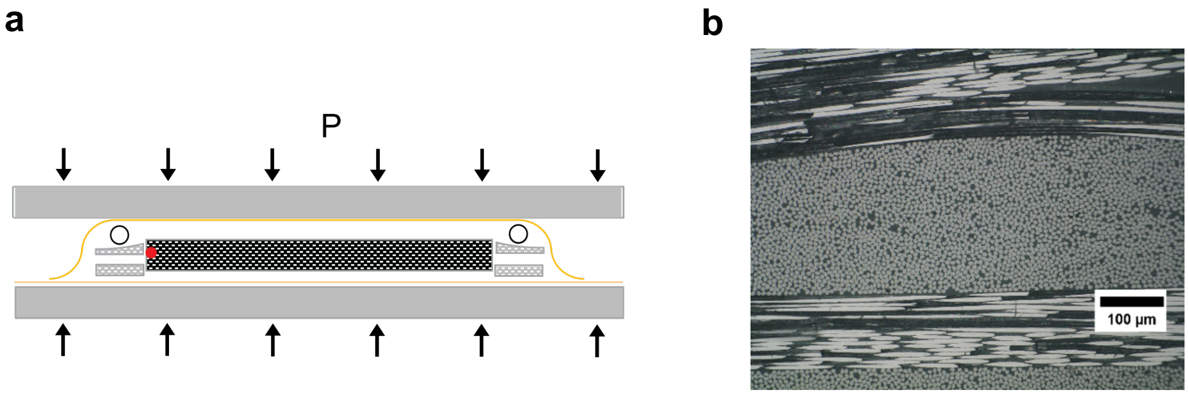

Figure 10. *a) Schematic of the high fiber volume fraction composite layup. b) Optical micrograph of composite sample at 500X magnification, demonstrating the high consolidation of the fabric preform.*

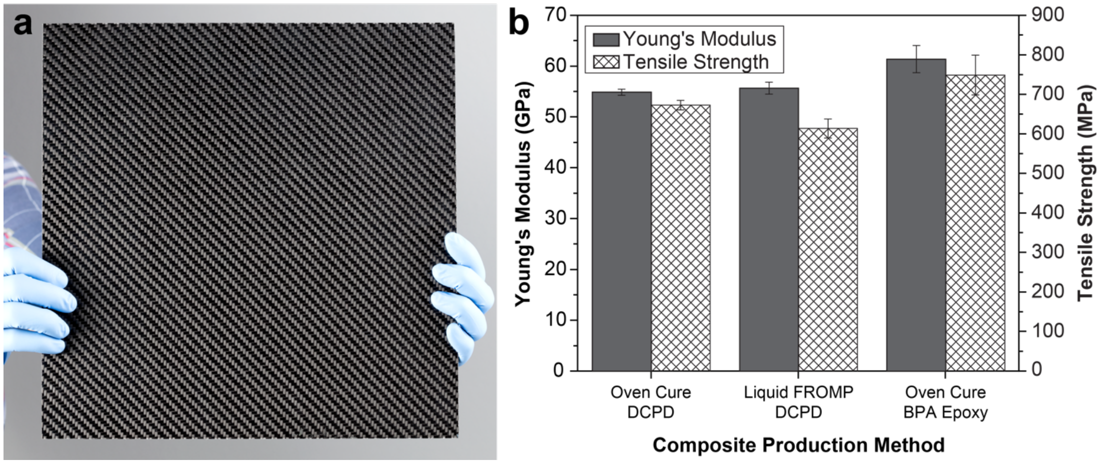

Figure 11. *a) FRPC produced by FP-DCPD. b) Mechanical properties of FRPCs produced through oven cure of DCPD, FP-DCPD, and oven cure of an aerospace-grade bisphenol A (BPA) epoxy.*

2.4 FP Freeform 4D Printing

By merging frontal polymerization (FP) with 3D printing, we were able to print and cure thermoset inks concurrently (Fig. 12). The inhibited DCPD gel is amenable to 3D printing, whereby the viscous gel is extruded from a print head and frontally polymerized immediately upon exiting the nozzle, allowing for the simultaneous free-form printing and curing of thermoset polymers. Matching the print head velocity to the front velocity allows for the manufacture of free-form complex architectures not possible with traditional additive manufacturing approaches (Fig. 12c). The polymerized segment of the filament structurally supports the printed part during its fabrication and no post-processing is required.

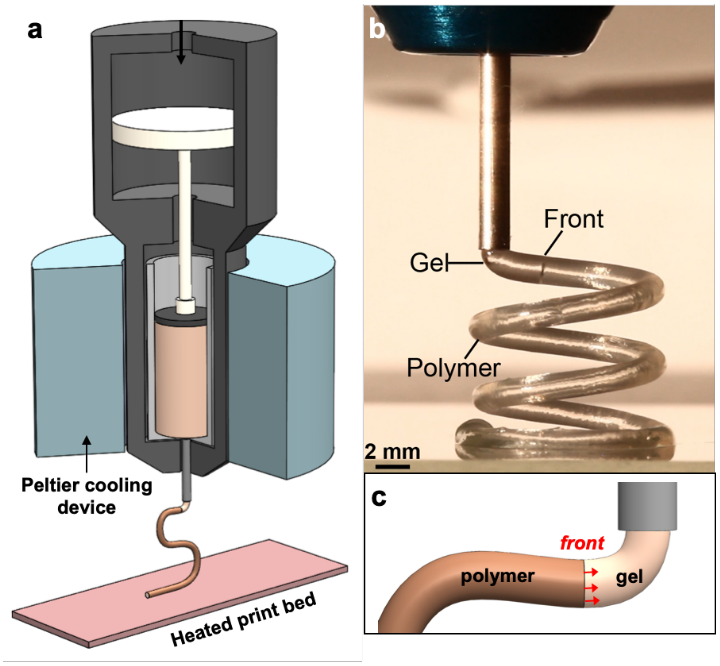

Fig. 12. *(a) Schematic of the 3D printing assembly. (b) FP free form printing of a helical geometry. (c) Zoomed image of FP front following the print nozzle [14].*

Unlike traditional direct ink writing, the filament is viscoelastic only for a small amount of time (≤ 10 s) and is rapidly solidified before any gravity-induced deflection can take place. We have successfully printed cantilever structures with unprecedented aspect ratios (length over diameter) of 115 (Fig. 13). Our technique has led to a marked improvement over current direct ink writing techniques, where aspect ratio values are less than 30 (6-8). The cross-section of the polymerized filament is shown in the inset of Fig. 13b, verifying that the filament retains a high degree of circularity. A range of free form objects were printed (Fig. 14).

Figure 13. *a) Schematic of printing behavior for frontally polymerizable ink. Soft gel extruded from the nozzle is immediately polymerized into a rigid thermoset by the front. b) Image of a spanning filament that is printed. The aspect ratio is 115. Inset shows the cross-section of a printed filament, which shows a high degree of circularity. Scale bar in the inset is 200 μm.*

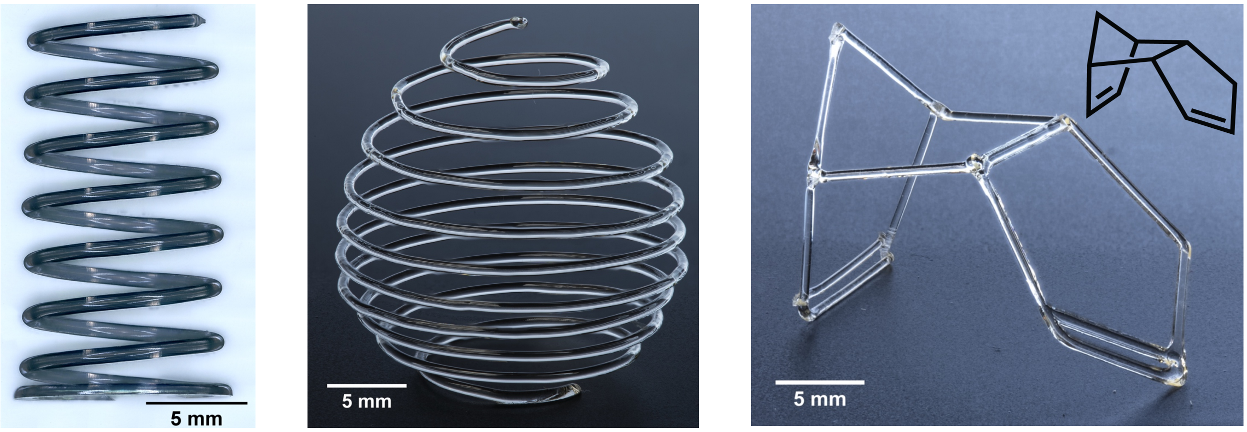

Spring helix

Ball helix

DCPD molecule

Figure 14. *Example of free form 3D printing by frontal polymerization of DCPD.*

2.5 Numerical Modeling of Rapid Polymerization Fronts

Our experiments were guided by the numerical modeling of the FP process, both in the neat DCPD resin as well as FPRC. We developed a nonlinear, transient finite element solution of the thermo-chemical reaction-diffusion equations that was implemented in the Multiphysics Object-Oriented Simulation Environment (MOOSE) to take advantage of the mesh adaptivity capabilities needed to capture the very sharp gradients in temperature and degree of cure present in the vicinity of the moving front [19]. We demonstrated the ability of the MOOSE framework to model FP in a channel of DCPD monomer and to capture the effect of a conductive fiber tow on the shape and speed of the front (Fig. 15). For the CFRP, we validated the thermo-chemical model through a detailed comparison between experimental measurements and numerical predictions of the dependence of the front velocity on fiber volume fraction, ϕ. The model was able to capture the initial increase in front speed with ϕ due to the higher thermal conductivity of the carbon fibers, followed by the steady decrease due to the reduction in the available heat of reaction as the relative portion of resin decreases with further increases in ϕ.

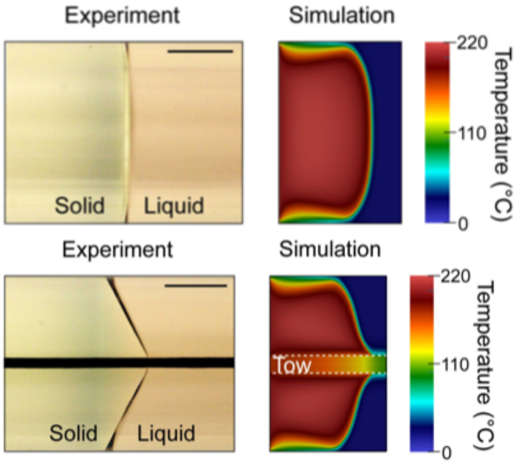

Figure 15. *Propagation of a polymerization front in DCPD captured experimentally and via simulation. The bottom row shows how the presence of a single carbon fiber tow affects the shape of the front (Scale bar is 4 mm).*

For modeling of composites, we developed a homogenized reaction-diffusion model to capture the propagation of a FP front in unidirectional composites and then extended the nonlinear, multi-physics finite element solver developed to solve the homogenized thermo-chemical model. The solver allows us to obtain the temperature and degree of cure profiles during the FP-based composites manufacturing process. Figure 16 shows the degree of cure and the normalized temperature profiles for unidirectional carbon fiber composites made with DCPD and loaded with 20% and 40% fibers, indicating the impact of carbon fibers on the speed and sharpness of the polymerization front. Profiles of the normalized temperature and degree of cure for the neat resin case (i.e., in the absence of fibers) are also included in this figure for comparison.

We then complemented the 1-D simulations with 2-D studies where heat losses from the composites layer to the surroundings are considered, as shown in Fig. 17 for the case of ϕ=0.3. By simulating a full sweep of fibers volume fractions in the unidirectional carbon/DCPD composites, two different regimes were revealed. In the first one, which corresponds to low values of the fiber volume fraction, the velocity of the polymerization front increases with the fiber volume fraction due to the contribution of the thermally conductive carbon fibers to the effective thermal conductivity of the composite. In the second regime, the front velocity decreases with increasing fiber volume fraction due to the increasing deficiency of monomer, which leads to a reduced heat source associated with the exothermic reaction.

To validate the model, unidirectional composite panels with varying fiber volume fraction were fabricated using an open molding system and frontal polymerization curing technique. Figure 18 presents a comparison between the experimental results (red square symbols) and the output of 1-D (black circles) and 2-D (blue triangles) numerical studies. With increasing fiber volume fraction ϕ, the experimental and 1D results diverge, indicating the need to include the effect of the boundary conditions in the 2D simulations. The 2-D results show a good match with the experimental measurements of the front velocity and a better prediction of the maximum temperature associated with the front. The temperature variation may be attributed to the position of thermocouples in the composite layup, which are located at the surface of the composites not at the center as in the simulations.

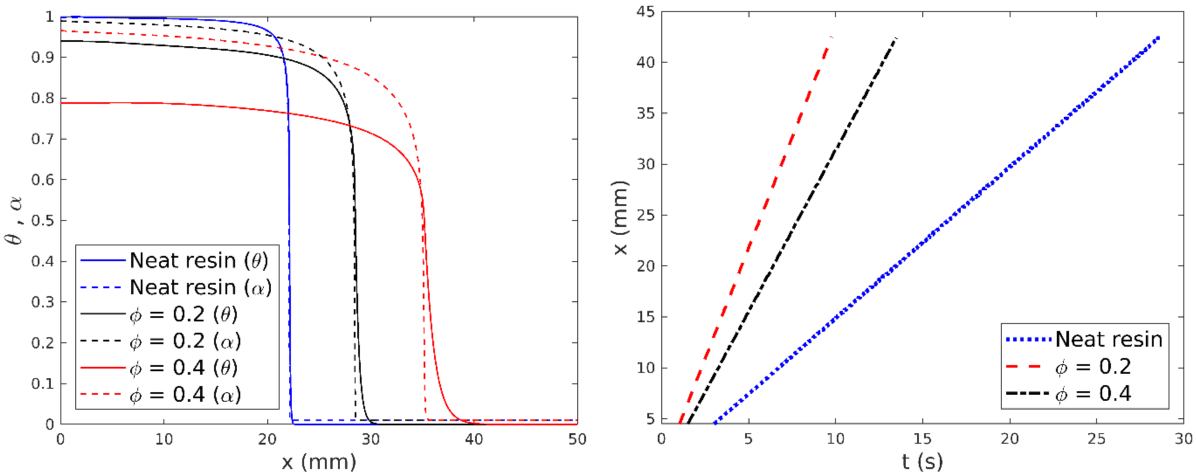

(a) (b)

Figure 16. *(a) Degree of cure and normalized temperature profiles and (b) front location versus time for three values of carbon fiber volume fraction: ϕ= 0.0, 0.2, and 0.4.*

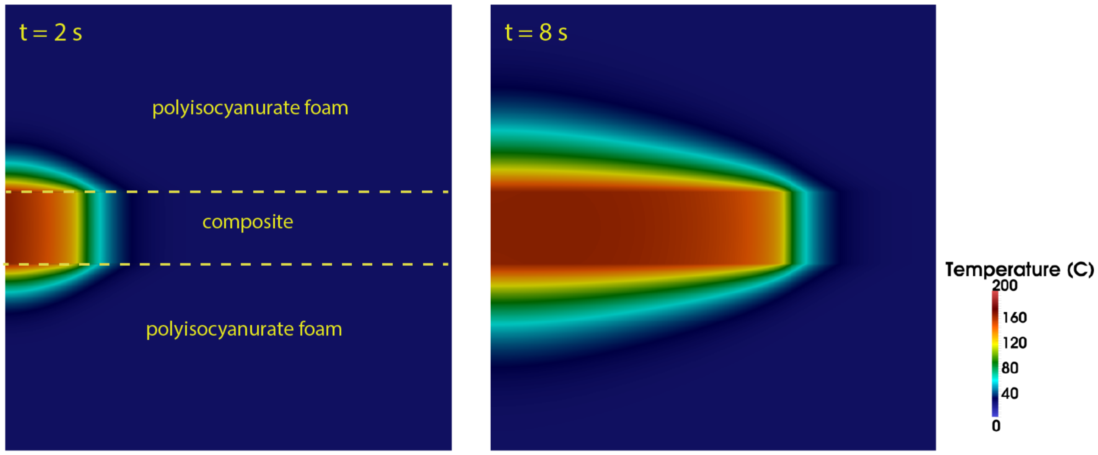

Figure 17*. Temperature contours predicted by 2-D model during front propagation for (a) t = 2 s and (b) t = 8 s, (ϕ = 0.3).*

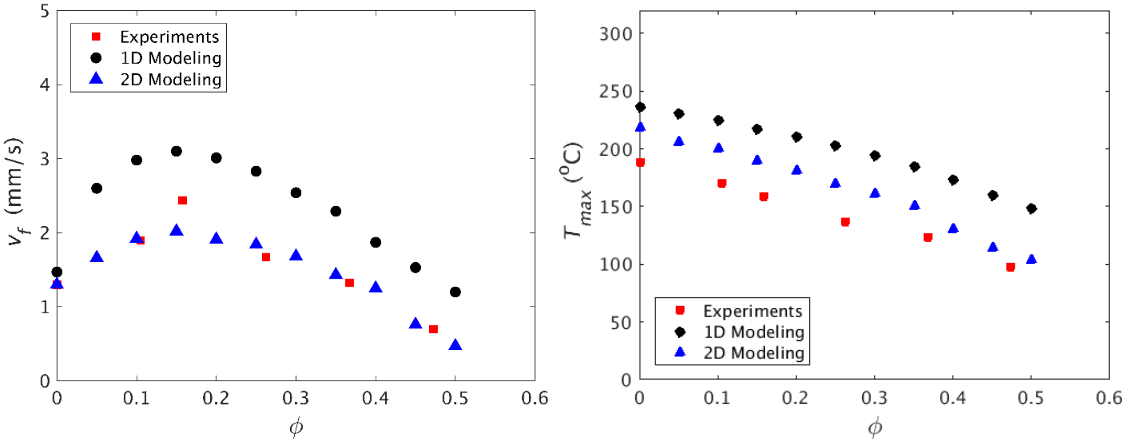

(a) (b)

Figure 18. *Model Validation: Comparison of the dependence of the front velocity (a) and maximum temperature (b) with respect to the fiber volume fraction ϕ obtained experimentally (square symbols) and numerically using the 1D (circles) and 2D (triangles) models.*

REFERENCES

1. J. F. Patrick, M. J. Robb, N. R. Sottos, J. S. Moore, S. R. White, Polymers with autonomous life-cycle control. *Nature* **540**, 363-370 (2016).

2. H. Mohapatra, M. Kleiman, A. P. Esser-Kahn, Mechanically controlled radical polymerization initiated by ultrasound. *Nat Chem* **9**, 135-139 (2017).

3. Z. H. Wang, X. C. Pan, J. J. Yan, S. Dadashi-Silab, G. J. Xie, J. N. Zhang, Z. H. Wang, H. S. Xia, K. Matyjaszewski, Temporal Control in Mechanically Controlled Atom Transfer Radical Polymerization Using Low ppm of Cu Catalyst. *Acs Macro Lett* **6**, 546-549 (2017).

4. T. G. McKenzie, E. Colombo, Q. Fu, M. Ashokkumar, G. G. Qiao, Sono-RAFT Polymerization in Aqueous Medium. *Angew Chem Int Edit* **56**, 12302-12306 (2017).

5. A. M. Parfitt, Osteonal and Hemi-Osteonal Remodeling - the Spatial and Temporal Framework for Signal Traffic in Adult Human Bone. *J Cell Biochem* **55**, 273-286 (1994).

6. A. R. Gilbert, S. W. Kantor, Transient Catalysts for the Polymerization of Organosiloxanes. *J Polym Sci* **40**, 35-58 (1959).

7. P. W. Zheng, T. J. McCarthy, A Surprise from 1954: Siloxane Equilibration Is a Simple, Robust, and Obvious Polymer Self-Healing Mechanism. *J Am Chem Soc* **134**, 2024-2027 (2012).

8. M. Kleiman, K. S. Brubaker, D. T. Nguyen, A. P. Esser-Kahn, Bio-Inspired Morphogenesis Using Microvascular Networks and Reaction-Diffusion. *Chem Mater* **27**, 4871-4876 (2015).

9. B. P. Krull, R. C. R. Gergely, W. A. S. Cruz, Y. I. Fedonina, J. F. Patrick, S. R. White, N. R. Sottos, Strategies for Volumetric Recovery of Large Scale Damage in Polymers. *Adv Funct Mater* **26**, 4561-4569 (2016).

10. S. R. White, J. S. Moore, N. R. Sottos, B. P. Krull, W. A. S. Cruz, R. C. R. Gergely, Restoration of Large Damage Volumes in Polymers. *Science* **344**, 620-623 (2014).

11. L. M. Dean, B. P. Krull, K. R. Li, Y. I. Fedonina, S. R. White, N. R. Sottos, Enhanced Mixing of Microvascular Self-Healing Reagents Using Segmented Gas-Liquid Flow. *ACS Appl Mater Inter* **10**, 32659-32667 (2018).

12. J. A. Pojman, V. M. Ilyashenko, A. M. Khan, Free-radical frontal polymerization: Self-propagating thermal reaction waves. *J Chem Soc Faraday T* **92**, 2825-2837 (1996).

13. J. A. Pojam, in *Polymer Science: A Comprehensive Reference*. (Elsevier BV, Amsterdam, 2012), pp. 957–980.

14. I. D. Robertson, M. Yourdkhani, P. J. Centellas, J. E. Aw, D. G. Ivanoff, E. Goli, E. M. Lloyd, L. M. Dean, N. R. Sottos, P. H. Geubelle, J. S. Moore, S. R. White, Rapid energy-efficient manufacturing of polymers and composites via frontal polymerization. *Nature* **557**, 223 (2018).

15. A. Mariani, S. Fiori, Y. Chekanov, J. A. Pojman, Frontal ring-opening metathesis polymerization of dicyclopentadiene. *Macromolecules* **34**, 6539-6541 (2001).

16. A. Ruiu, D. Sanna, V. Alzari, D. Nuvoli, A. Mariani, Advances in the Frontal Ring Opening Metathesis Polymer

17. I. D. Robertson, L. M. Dean, G. E. Rudebusch, N. R. Sottos, S. R. White, J. S. Moore, Alkyl Phosphite Inhibitors for Frontal Ring-Opening Metathesis Polymerization Greatly Increase Pot Life. *Acs Macro Lett* **6**, 609-612 (2017).

18. Liu, H., Wei, H. and Moore, J.S., Frontal Ring-Opening Metathesis Copolymerization: Deviation of Front Velocity from Mixing Rules, *ACS Macro Letters*, 8, 846-851 (2019)

19. E. Goli, I. D. Robertson, P. H. Geubelle, J. S. Moore, Frontal Polymerization of Dicyclopentadiene: A Numerical Study. *J Phys Chem B* **122**, 4583-4591 (2018).